

Medium Energy Ion Scattering Spectrometry of Spinel Structure of $\text{Li}_4\text{Ti}_5\text{O}_{12}$ Surface

Haitham M. Abd ¹, Layla A.H. Flayeh ¹, Sabah N. Abas ²

¹ Department of Physics, College of Science, University of Dhi Qar, Al-Nasiriyah, IRAQ

² Department of Physics, College of Education for Pure Sciences, University of Dhi Qar, Al-Nasiriyah, IRAQ

Abstract

Spinel lithium titanate ($\text{Li}_4\text{Ti}_5\text{O}_{12}$) is one of the promising anode materials for high-performance lithium-ion batteries (LIBs). It is crucial to investigate atomistic structures of $\text{Li}_4\text{Ti}_5\text{O}_{12}$ surfaces to understand the phenomena at the LTO/electrolyte interfaces such as CO_2 -gas generation which greatly affects the performance and safety of LIBs. By applying scanning tunneling microscopy (STM) and medium energy ion scattering (MEIS) to a $\text{Li}_4\text{Ti}_5\text{O}_{12}$ (111) film prepared from a TiO_2 wafer, we found that there exists two kinds of Li-terminated (111) terraces bounded by steps with different heights. In the major terraces, the top hexagonal Li layer is stacked above the oxygen layer, while the top Li layer is stacked above the Ti-Li layer in the minor terraces. The relative stability between the two surface structures seems to depend on the atmosphere due to different stoichiometry, which is a possible origin of CO_2 generation via redox interaction with electrolyte molecules.

Keywords: $\text{Li}_4\text{Ti}_5\text{O}_{12}$; Spinel structures; Scanning tunneling microscopy; MEIS

Received: 2 August 2024; **Revised:** 3 September 2024; **Accepted:** 10 September 2024; **Published:** 1 October 2024

1. Introduction

Lithium transition-metal oxides [1-3] are widely used as active electrode materials for lithium-ion batteries (LIBs) due to their reversible lithium insertion/extraction properties. Especially, the spinel lithium titanium oxide ($\text{Li}_4\text{Ti}_5\text{O}_{12}$, LTO) [3] is one of the most important anode materials for its high rate Li insertion/extraction (charge-discharge) capability [4,5] with excellent durability [6]. These properties, based on the rigid lattice stability of the spinel framework [3-5], enable the design of a safer anode of LIBs than a carbon-based one, promising for the usage in electric vehicles and other wide industrial applications [7]. Numerous studies have been performed on the $\text{Li}_4\text{Ti}_5\text{O}_{12}$ bulk structure and its changes by Li insertion/extraction [8-13], while the $\text{Li}_4\text{Ti}_5\text{O}_{12}$ surface structure has not yet been understood. The Li insertion/extraction occurs via the $\text{Li}_4\text{Ti}_5\text{O}_{12}$ /electrolyte interface, and the interface phenomena such as CO_2 -gas generation [14,15] of $\text{Li}_4\text{Ti}_5\text{O}_{12}$ in high-power LIBs. Therefore, the investigation of atomistic $\text{Li}_4\text{Ti}_5\text{O}_{12}$ surface structure is essential to understand the atomistic mechanisms of electrochemical processes and various phenomena

at $\text{Li}_4\text{Ti}_5\text{O}_{12}$ /electrolyte interfaces [16-18], seriously affecting the performance and safety of LIBs. Except for graphite electrodes, there are few reports on atomic scale structures of surfaces of electrode materials, because of the difficulty in preparing crystalline samples with atomically-flat surfaces suitable for scanning-probe microscopy (SPM). Recently, we developed the technique to prepare $\text{Li}_4\text{Ti}_5\text{O}_{12}$ films with atomically-flat surfaces on a TiO_2 wafer using conventional solid-state reaction [19]. The prepared $\text{Li}_4\text{Ti}_5\text{O}_{12}$ film was shown to have electrochemical activity essentially similar to usual $\text{Li}_4\text{Ti}_5\text{O}_{12}$ power. For the film sample, the morphology changes of a $\text{Li}_4\text{Ti}_5\text{O}_{12}$ (111) surface in the early stage of initial Li insertion process [20] were investigated by using atomic force microscopy (AFM).

In the present study, we investigated the atomic scale structure of a $\text{Li}_4\text{Ti}_5\text{O}_{12}$ (111) surface by using high-resolution scanning tunneling microscopy (STM). We also apply medium energy ion scattering (MEIS) analysis, which can provide complementary information on the elemental depth profile in the surface and sub-surface layers. Atomic models from

the experimental results are discussed from the viewpoints of surface stoichiometry and surface electronic structure.

2. Experimental Part

A $\text{Li}_4\text{Ti}_5\text{O}_{12}$ thin-film sample was prepared by solid state reaction as previously reported [19]. A commercial rutile- $\text{TiO}_2(111)$ wafer (SHINKOSHA, Co. LTD) was cleaned in analytical grade acetone by an ultrasonic cleaner to remove surface contaminations. The wafer with a size of $2 \times 6 \times 0.5$ mm was sealed in a 99% alumina crucible with 1 mg of $\text{LiOH} \cdot \text{H}_2\text{O}$ and calcined for 15 h at 1173 K in air. In the calcination process, LiOH is vaporized, and a single-crystalline $\text{Li}_4\text{Ti}_5\text{O}_{12}$ film with about 15 μm thickness is grown on the $\text{TiO}_2(111)$ surface. The crystal structure of the grown film was evaluated by a Mo- $\text{K}\alpha$ X-ray diffractometer (X'Pert PRO, PANalytical) with out-of-plane measurement. AFM (NanoNavi-II, SIL) was performed by dynamic force mode in air at 1000 nm^2 area. We observed the surface structure in an atomic scale with high-resolution STM (JSTM-4500TX, JEOL) under ultra-high vacuum (UHV, $\sim 10^{-7}$ Pa) at room temperature. Before the STM observation, the sample was heated by silicone heat board at 1073 K for 1 h and 1123 K for 15 min under the UHV to prepare the clean surface. STM images were acquired at +1 to +1.5 V of sample bias and 0.3 nA of tunneling current. High-resolution MEIS using 80 keV He^+ ions allowed for elemental depth profiling, which was carried out at beam-line 8 named SORIS at Ritsumeikan SR Center. Prior to the MEIS analysis, we heated the sample at 923 K for 1 h and then at 1123 K for 15 min in UHV and confirmed no carbon contamination by Auger electron spectroscopy (see Fig. 1).

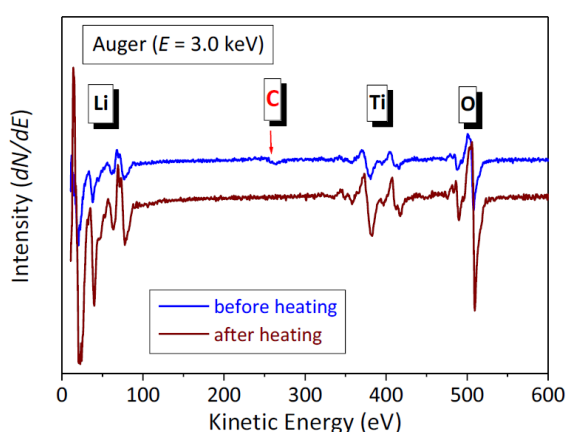


Fig. (1) Auger spectra taken for the sample before (blue) and after heating in UHV

3. Results and Discussion

Here, we explain the (111) atomic-layer stacking in a spinel $\text{Li}_4\text{Ti}_5\text{O}_{12}$ crystal ($Fd\bar{3}m$, $a = 0.8357$ nm [21]) before reporting experimental results. Figure 2(a) shows four kinds of (111) atomic layers. Li atoms at the 8a sites of Wyckoff positions form the

8a (Li) layer (indicated by a red solid line), and O atoms at the 32e sites form the 32e (O) layer (indicated by a black solid line). The 16d-1 ($\text{Li}_{1/6}\text{Ti}_{5/6}$) and 16d-2 ($\text{Li}_{1/6}\text{Ti}_{5/6}$) layers (indicated by blue and green solid lines) consist of Li and Ti atoms with the ratio of 1:5 at the 16d sites. As shown in Fig. (2b), the in-plane atomic density is equal to that of the 8a (Li) and 16d-1 ($\text{Li}_{1/6}\text{Ti}_{5/6}$) layers, while it is three times larger that of the 16d-2 ($\text{Li}_{1/6}\text{Ti}_{5/6}$) layer and four times larger that of the 32e (O) layer. The 8a (Li) and 16d-1 ($\text{Li}_{1/6}\text{Ti}_{5/6}$) layers should have hexagonal atomic arrangements with the interatomic distance of about 0.6 nm, while the minimum interatomic distance in the 16d-2 ($\text{Li}_{1/6}\text{Ti}_{5/6}$) layer is about 0.3 nm. Note that the distinction between Ti and Li atoms on the 16d-1 and 16d-2 layers is not definite essentially, while only the ratio of 1(Li):5(Ti) is definite. In the (111) stacking sequence in Fig. (2a), total six layers as two 8a (Li), two 32e (O), one 16d-1 and one 16d-2 layers, constitute one period.

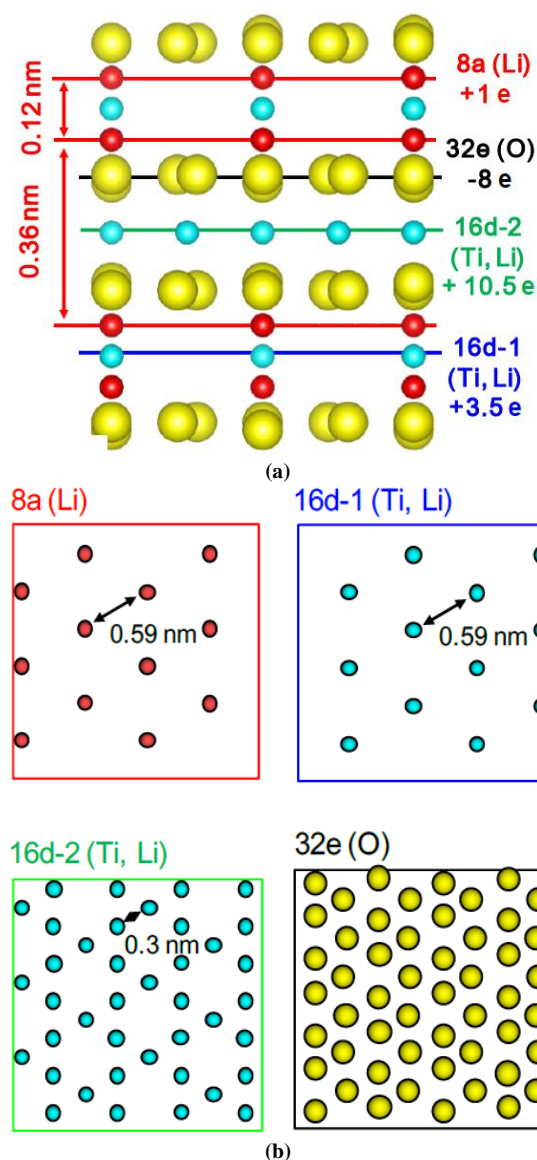


Fig. (2) (a) Out-of-plane structure of (111) layer stacking in $\text{Li}_4\text{Ti}_5\text{O}_{12}$ viewed from [112] direction. Formal ionic charges of each atomic layer per 1×1 period are denoted. (b) In-plane atomic arrangements of four kinds of (111) layers shown in (a). Values of intervals between the 8a (Li) layers and interatomic distances in the hexagonal atomic arrangements are estimated from the $\text{Li}_4\text{Ti}_5\text{O}_{12}$ crystal structure with the experimental lattice constant of $a = 0.8357 \text{ nm}$ [21]

From the crystallographic data of the bulk $\text{Li}_4\text{Ti}_5\text{O}_{12}$ [21], it can be said that only the 8a (Li) layers are repeated with the two kinds of intervals as about 0.12 and 0.36 nm. In Fig. (2a), a formal ionic charge of each (111) atomic layer per 1×1 hexagonal period is also denoted. This is obtained by the sum of charges of each species as $+1e + 4e$ (Ti) and $2e$ (O) on each layer. It can be said that each oxygen layer with $8e$ (four oxygen atoms per 1×1 period) receives $5.25e$ from the lower 16d-2 ($\text{Li}_{1/6}\text{Ti}_{5/6}$) layer and $2.75e$ from the upper 8a (Li) and 16d-1 ($\text{Li}_{1/6}\text{Ti}_{5/6}$) layers.

In Fig. 3(a), the out-of-plane X-ray (Mo-K α) diffraction spectrum of the prepared film reveals strong and sharp diffraction lines of the $\text{Li}_4\text{Ti}_5\text{O}_{12}$ (111) series, indicating that the prepared film is highly-ordered (111) crystalline film. Fig. 3(b) shows the AFM image of the prepared (111) film surface. We can see clear steps with a single atomic-layer height of 0.48 nm and atomically-flat terraces with $R_a = 0.02 \text{ nm}$ of surface roughness. This step height corresponds to one period of the sequence of (111) atomic layers in Fig. 2(a).

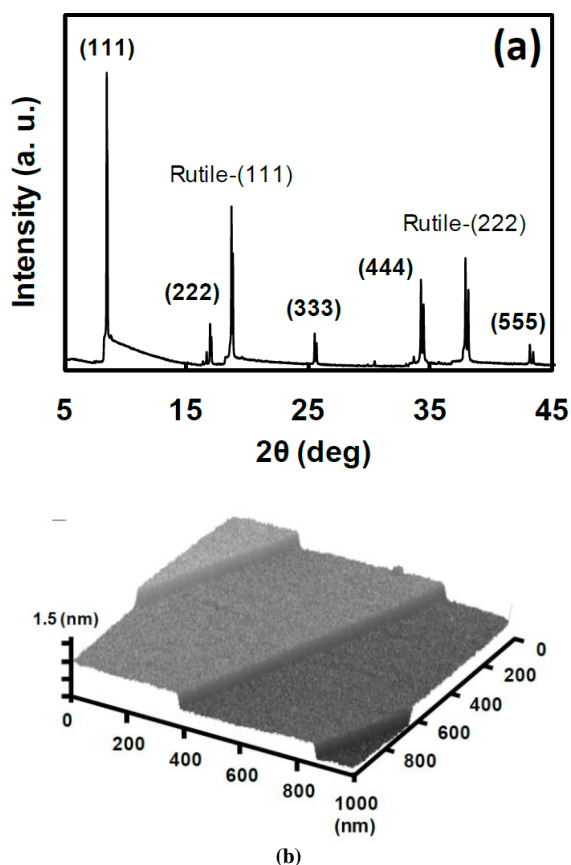


Fig. (3) (a) Out-of-plane X-ray diffraction spectrum of the prepared $\text{Li}_4\text{Ti}_5\text{O}_{12}$ film. (b) AFM image of the prepared $\text{Li}_4\text{Ti}_5\text{O}_{12}$ (111) surface acquired from $1000 \times 1000 \text{ nm}$ scan area

Figure 4(a) shows the STM image of the $\text{Li}_4\text{Ti}_5\text{O}_{12}$ (111) surface acquired from $50 \times 50 \text{ nm}$ area, where we can see clear steps and terraces with some atomistic defects. This image is not the periodic one of some artifact, but is the true image of atomic scale resolution. Figure 4(b) shows the surface height profile of X-Y line across the two steps in Fig. 4(a). The heights of the two steps are 0.35 and 0.13 nm. This indicates the presence of two kinds of different (111) terraces, in contrast to the AFM results of the single step height of 0.48 nm in Fig. 3(b), indicating only one type of (111) terrace. Figure 4(c) shows the high-resolution STM image acquired from the square area in the upper terrace in Fig. 4(a). We can see a hexagonal arrangement of bright spots with intervals of about 0.6 nm, while there also seem to exist some defects. A similar hexagonal arrangement of spots with similar intervals is also observed on the middle and lower terraces in Fig. 4(a).

The observed hexagonal atomic arrangement of bright spots on each terrace indicates that the top layers of the two kinds of terraces should be 8a (Li) or 16d-1 ($\text{Li}_{1/6}\text{Ti}_{5/6}$) layers shown in Fig. (2b), having a similar hexagonal atomic arrangement with interatomic distance of about 0.6 nm.

From the step heights, we can expect that both kinds of terraces are Li-terminated surfaces as the type (A) and type (B) surfaces shown in Fig. (5). The upper terrace in Fig. (4a) should consist of the 8a (Li) layer stacked on the 32e (O) layer (type (B)), while the middle terrace should consist of the 8a (Li) layer stacked on the 16d-1 ($\text{Li}_{1/6}\text{Ti}_{5/6}$) layer (type (A)). Only this combination can satisfy the relation between the observed step heights (0.13 nm and 0.35 nm) and the intervals between the atomic layers in Fig. (2a) within the models of the (111) atomic-layer sequence similar to the bulk. It is apparent that the two models of the Li-terminated surfaces in Fig. 5 have different chemical compositions (stoichiometry) in the surface regions. As analyzed later, the type (B) surface is oxygen-rich and the type (A) surface is oxygen-deficient. Thus it is natural that the two kinds of the Li-terminated surfaces have different stabilities depending on the atmosphere, namely the oxygen chemical potential, as analyzed by Gibbs free energies.

In order to prove the present atomic models of the two kinds of (111) terraces, we have performed the high-resolution MEIS observation. This technique can identify a target atomic mass M with a resolution of $\Delta M/M \sim 1/100$ and provide valuable information on the atomic species and their arrangement in the surface and sub-surface layers.

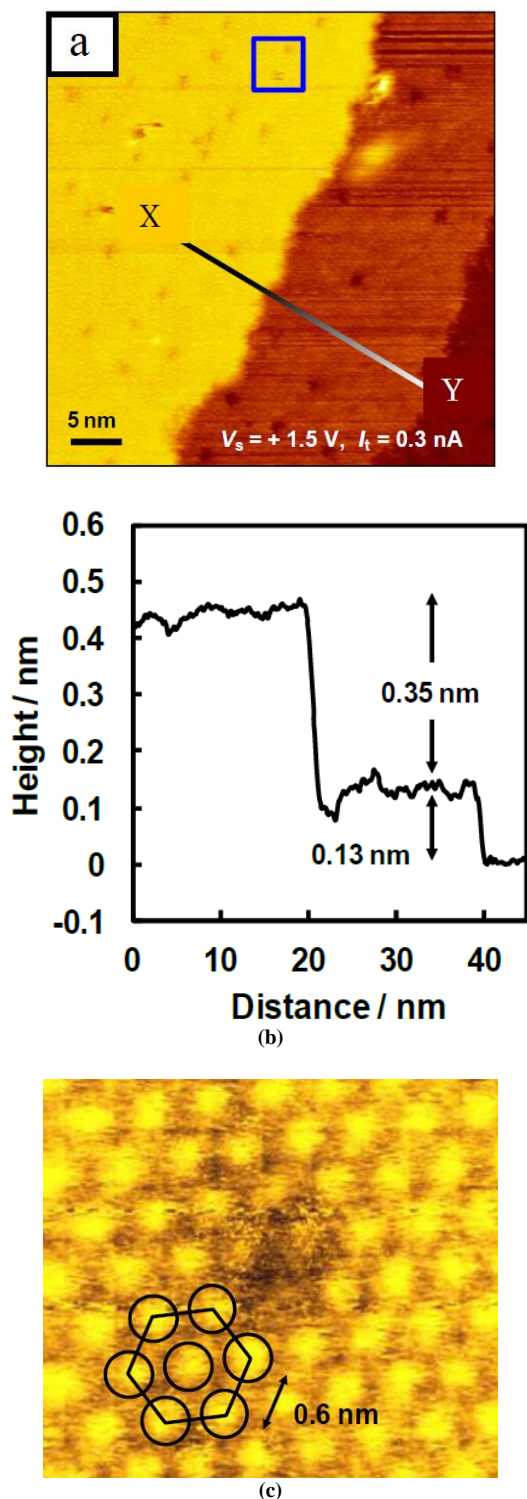


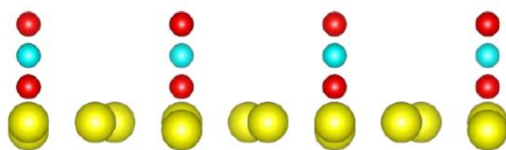
Fig. (4) (a) Atomic scale image of the $\text{Li}_4\text{Ti}_5\text{O}_{12}$ (111) surface acquired by UHV-STM (JEOL-4500TX). (b) Surface height profile of X-Y line shown in (a). (c) Magnified STM image of the $\text{Li}_4\text{Ti}_5\text{O}_{12}$ (111) surface acquired from the square area in (a)

The details of MEIS analysis were described elsewhere [22,23]. The sample was prepared in the same manner as described for the STM observation and thus annealed at 923K for 1 h and then at 1123K for 15 min in UHV, resulting in complete

elimination of carbon contaminations, as indicated in Fig. (1). Figure 6 shows the MEIS spectrum (open circles) observed for 80 keV He^+ ions incident on the clean $\text{Li}_4\text{Ti}_5\text{O}_{12}$ (111) surface and scattered from the Ti atoms. The vertical arrow in this figure indicates the energy position of He^+ ions scattered from Ti atoms on top of the surface assumed to exist. The slightly lower energy shift of the leading edge (mid energy position of the slope) suggests the presence of a few over-layers consisting of low Z-number atoms above the Ti atoms. In other words, there are no Ti atoms on top of any terraces of the $\text{Li}_4\text{Ti}_5\text{O}_{12}$ (111) surface. The blue and red solid lines in Fig. 6 show the simulated spectra assuming the type (A) and type (B) surfaces, respectively. The small surface peak appearing at 67.5 keV in the blue line comes from the 16d-1 ($\text{Li}_{1/6}\text{Ti}_{5/6}$) layer below the 8a (Li) layer in the type (A) surface. In contrast, for the type (B) surface, the presence of two over-layers, the 8a (Li) and 32e (O) layers, smears out such a surface peak from the 16d-2 ($\text{Li}_{1/6}\text{Ti}_{5/6}$) layer, because of increased energy loss and straggling for He^+ ions subjected during passing through the over-layers. Note that the energy loss and straggling are caused by the interactions between He^+ ions and target electrons and thus lower Z-number materials give lower energy loss and straggling. It is clear that the type (B) surface structure gives the best-fit to the observed MEIS spectrum. However, the MEIS results do not necessarily rule out the possibility of the coexistence of the type (A) surface as the minority portion of terraces. In Fig. (6), the green line shows the simulated spectrum for the 1:1 mixture of the type (A) and type (B) surfaces, where the effect of the type (A) surface is observed as a small shoulder. Also in the experimental spectrum, there seems to exist a very small shoulder, while it might be caused by some kind of errors or fluctuations. We have also performed simulations for smaller portions of the type (A) surface less than 50%, which indicates no clear effects in the simulated spectra from the coexistence of the type (A) surface less than ~20 %. Thus the MEIS results cannot exclude the possibility of the coexistence of the type (A) surface less than 20% for the sample analyzed by MEIS.

The present MEIS result indicating that the type (B) surface is a large majority in the sample surface is consistent with the fact that the area of the type (B) surface as the upper terrace is much wider than the area of the type (A) surface as the middle terrace in the STM image of Fig. (4a), and the fact that occasionally only one type of the (111) terrace, probably the type (B) structure, with the single step height of 0.48 nm is observed in the STM image. Note that the high-temperature treatment in UHV for the MEIS sample is similar to the sample observed by STM.

(a) : 8a Li on 16d-1 layer (+2.75 e)



(b) : 8a Li on 32e layer (-1.75 e)

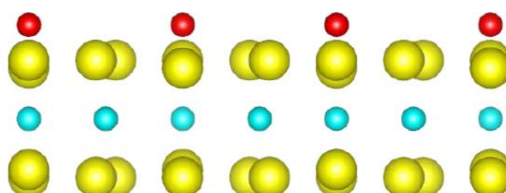


Fig. (5) Side views of two types of Li-terminated $\text{Li}_4\text{Ti}_5\text{O}_{12}$ (111) surfaces seen from the [112] direction. Red, blue and yellow circles denote, respectively lithium, titanium and oxygen atoms

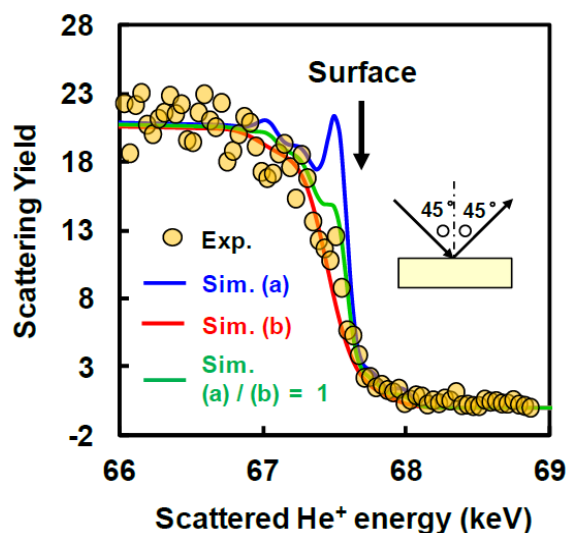


Fig. (6) MEIS spectrum observed for 80keV He^+ ions incident on the $\text{Li}_4\text{Ti}_5\text{O}_{12}$ (111) surface at 45° with respect to surface normal and scattered to 45° from Ti atoms. Blue, red and green curves are simulated MEIS spectra assuming type (A), type (B) and their 1:1 mixed surfaces, respectively

The present models of two kinds of Li-terminated surfaces have the sequence of (111) atomic-layer stacking similar to the bulk. Of course, we do not deny general possibilities of further reconstruction in in-plane or stacking structure at the surface. The present experimental results of step heights, periodic bright spots in STM images and MEIS naturally leads to the present models and we did not obtain any results indicating further reconstruction. About cation termination in stable oxide surfaces in usual atmosphere, note that there exist a lot of examples similar to the present type (B)

structure, such as spinel $\text{Co}_3\text{O}_4(111)$ and $\text{Fe}_3\text{O}_4(111)$ surfaces [24-28] and corundum $\text{Al}_2\text{O}_3(0001)$ surface [29], where the cation topmost layer is stacked above the surface oxygen layer with the atomic-layer stacking sequence similar to the bulk. A recent study of the $\text{Li}_2\text{TiO}_3(001)$ surface with components similar to $\text{Li}_4\text{Ti}_5\text{O}_{12}$ has also concluded the cation (Li^+) termination from the results of STM observation and classical molecular dynamics simulations[30]. Similarly, we think that unoccupied orbitals at surface cations (Li^+) on the type (B) surface should be concerned with bright spots in the STM image.

4. Conclusions

We investigated the atomistic structure of a $\text{Li}_4\text{Ti}_5\text{O}_{12}$ (111) surface by means of STM, AFM and MEIS analyses. In the STM, there are two kinds of (111) surface terraces with apparent hexagonal atomic arrangements with interatomic distance of 0.6 nm, bounded by steps with two different step heights. We propose that the major portion of the terraces is an oxygen-rich surface, consisting of the sequence as $8a(\text{Li})/32e(\text{O})/16d-2(\text{Li}_{1/6}\text{Ti}_{5/6})/32e(\text{O})$ and that the minor portion of the terraces is a cation-rich surface, consisting of the sequence of $8a(\text{Li})/16d-1(\text{Li}_{1/6}\text{Ti}_{5/6})/8a(\text{Li})/32e(\text{O})$. The present view was clearly supported by the MEIS analysis to provide reliable information on the T-atom distribution in the surface and sub-surface layers. The major oxygen-rich $\text{Li}_4\text{Ti}_5\text{O}_{12}$ surface should have electronic holes, which is a possible origin of the CO_2 -gas generation via redox interaction with electrolyte molecules.

References

- [1] K. Mizushima, P.C. Jones, P.J. Wiseman, J.B. Goodenough, Mater. Res. Bull. 2 (1980) 112.
- [2] M.M. Thackeray, W.I.F. David, P.G. Bruce, J.B. Goodenough, Mater. Res. Bull. 18 (1983) 461.
- [3] T. Ohzuku, A. Ueda, Y. Yamamoto, J. Electrochem. Soc. 142 (1995) 1431.
- [4] S. Takai, M. Kamata, S. Fujine, K. Yoneda, K. Kanda, T. Esaka, Solid State Ionics 123 (1999) 165.
- [5] K. Ariyoshi, R. Yamato, T. Ohzuku, Electrochim. A. 51 (2005) 1125.
- [6] H.M. Wu, I. Belharouak, H. Deng, A. Abouimrane, Y.-K. Sun, K. Amine, J. Electrochem. Soc. 156 (2009) A1047.
- [7] N. Takami, H. Inagaki, T. Kishi, Y. Harada, Y. Fujita, K. Hoshina, J. Electrochem. Soc. 156 (2009) A128.
- [8] F. Ronci, P. Reale, B. Scrosati, S. Panero V. Rossi Albertini, P. Perfetti, M. di Michiel, J.M. Merino, J. Phys. Chem. B 106 (2002) 3082.
- [9] L. Aldon, P. Kubiak, M. Womes, J.C. Jumas, J. Olivier-Fourcade, J.L. Tirado, J.I. Corredor, C. Pérez Vicente, Chem. Mater. 16 (2004) 5721.
- [10] S. Scharner, W. Weppner, P. Schmid-Beurmann, J. Electrochem. Soc. 146 (1999) 857.

- [11] K. Kataoka, Y. Takahashi, N. Kijima, H. Hayakawa, J. Akimoto, K. Oshima, *Solid State Ionics* 180 (2009) 631.
- [12] S. Pyun, S.-W. Kim, H.-C. Shin, *J. Power Sources* 81 (1999) 248.
- [13] J.-F. Colin, V. Godbole, P. Novák, *Electrochem. Commun.* 12 (2010) 804.
- [14] I. Belharouak, G.M. Koenig, T. Tan, H. Yumoto, N. Ota, K. Amine, *J. Electrochem. Soc.* 159 (2012) A1165.
- [15] K. Wu, J. Yang, Y. Zhang, C. Wang, D. Wang, *J. Appl. Electrochem.* 42 (2012) 989.
- [16] M. Hirayama, H. Ido, K. Kim, W. Cho, K. Tamura, J. Mizuki, R. Kanno, *J. Am. Chem. Soc.* 132 (2010) 15268.
- [17] S.E. Sloop, J.B. Kerr, K. Kionoshita, *J. Power Sources* 119-121 (2003) 330.
- [18] R. Dedryvère, D. Foix, S. Franger, S. Patoux, L. Daniel, D. Gonbeau, *J. Phys. Chem. C* 114 (2010) 15268.
- [19] M. Kitta, T. Akita, Y. Maeda, M. Kohyama, *Appl. Surf. Sci.* 258 (2012) 3147.
- [20] M. Kitta, T. Akita, Y. Maeda, M. Kohyama, *Lanumuir* 28 (2012) 12384.
- [21] K. Kataoka, Y. Takahashi, N. Kijima, J. Akimoto, K. Ohshima, *J. Phys. Chem. Solids* 69 (2008) 1454.
- [22] Y. Kido, T. Koshikawa, *J. Appl. Phys.* 67 (1990) 187.
- [23] A. Ikeda, K. Sumitomo, T. Nishioka, Y. Kido, *Nucl. Instrum. Methods B* 115 (1996) 34.
- [24] M. Ritter, W. Weiss, *Surf. Sci.* 432 (1999) 81.
- [25] J. Ahdjoudj, C. Martinsky, C. Minot, M.A. Van Hove, G.A. Somorjai, *Surf. Sci.* 443 (1999) 133.
- [26] M.E. Grillo, M.W. Finnis, W. Ranke, *Phys. Rev. B* 77 (2008) 075407.
- [27] X.-L. Xu, Z.-H. Chen, Y. Li, W.-K. Chen, J.-Q. Li, *Surf. Sci.* 603 (2003) 653.
- [28] W. Meyer, K. Biedermann, M. Gubo, L. Hammer, K. Heinz, *J. Phys. Condens. Mater.* 20 (2008) 265011.
- [29] X.G. Wang, A. Chaka, M. Scheffler, *Phys. Rev. Lett.* 84 (2000) 3650.
- [30] K. Azuma, C. Dover, D.C. Grinter, R. Grau-Crespo, N. Almora-Barrios, G. Thornton, T. Oda, S. Tanaka, *J. Phys. Chem. C* 117 (2013) 5126.
- [31] R. Benedek, M.M. Thackeray, *Phys. Rev. B* 83 (2011) 165439.
- [32] P.M. Kowalski, B. Meyer, D. Marx, *Phys. Rev. B* 79 (2009) 115410.
- [33] Y.-B. He, B. Li, M. Liu, C. Zhang, W. Lv, C. Yang, J. Li, H. Du, B. Zhang, Q.-H. Yang, J.-K. Kim, F. Kang, *Scientific Reports* 2, 2013. <http://dx.doi.org/10.1038/srep00913> No. 913.
- [34] O.A. Hamadi, K.Z. Yahya and O.N.S. Jassim, *J. Semicond. Sci. Technol.*, 5(3) 182-186 (2005).
- [35] K.S. Khashan and O.A. Hamadi, *Eng. Technol. J.*, 25(2) 168-175 (2007).
- [36] O.A. Hamadi, *Iraqi J. Appl. Phys. Lett.*, 1(2) 3-8 (2008).
- [37] O.A. Hamadi, B.A.M. Bader and A.K. Yousif, *Eng. Technol. J.*, 26(8) 995-1001 (2008).
- [38] A.A. Hadi and O.A. Hamadi, *Iraqi J. Appl. Phys. Lett.*, 1(2) 23-26 (2008).
- [39] A.K. Yousif and O.A. Hamadi, *Bulg. J. Phys.*, 35(3) 191-197 (2008).
- [40] O.A. Hamadi, N.J. Shakir, F.H. Hussain, *Bulg. J. Phys.*, 37(4), 223-231 (2010).
- [41] O.A. Hamadi, *Iraqi J. Appl. Phys. Lett.*, 3(1) 23-26 (2010).
- [42] O.A. Hammadi and N.E. Naji, *Iraqi J. Appl. Phys.*, 10(2) 27-31 (2014).
- [43] O.A. Hammadi, W.N. Raja, M.A. Saleh and [44] W.A. Altun, *Iraqi J. Appl. Phys.*, 12(3), 35-42 (2016).
- [45] O.A. Hammadi, W.N. Raja, M.A. Saleh and W.A. Altun, *Iraqi J. Appl. Phys.*, 12(4), 19-28 (2016).
- [46] O.A. Hammadi, *J. Optoelectron. Phot.*, 7(5), 21 (2016).
- [47] O.A. Hammadi, *J. Laser Micro/Nanoeng.*, 11(6), 151 (2016).
- [48] O.A. Hammadi, *J. Biomed. Nanotechnol.*, 12(8), (2016).
- [49] O.A. Hamadi, *Iraqi J. Appl. Phys.*, 12(2) 9-13 (2016).
- [50] O.A. Hammadi, *Photonic Sensors*, 6(4) 345-350 (2016). DOI: 10.1007/s13320-016-0338-4
- [51] O.A. Hammadi and N.E. Naji, *Photonic Sensors*, 8(1) 43-47 (2018).